Formation of Interacting Spins on Flavosemiquinone and Tyrosine Radical in Photoreaction of a Blue Light Sensor BLUF Protein TePixD[†]

Hiroko Nagai,[‡] Yoshimasa Fukushima,[‡] Koji Okajima,[§,||] Masahiko Ikeuchi,[§] and Hiroyuki Mino*[,‡]

Division of Material Science (Physics), Graduate School of Science, Nagoya University, Furocho, Chikusa, Nagoya 464-8602, Japan, Department of Life Science (Biology), Graduate School of Arts and Science, University of Tokyo, Komaba 3-8-1, Meguro, Tokyo 153-8902, Japan, and Department of Biological Science, Graduate School of Science, Osaka Prefecture University, 1-1, Gakuen-cho, Sakai, Osaka 599-8531, Japan

Received May 30, 2008; Revised Manuscript Received October 7, 2008

ABSTRACT: Light-induced radicals were detected by electron paramagnetic resonance (EPR) and pulsed electron−nuclear double resonance (ENDOR) in the BLUF-domain protein TePixD of the thermophilic cyanobacterium *Thermosynechococcus elongatus* BP-1. The illumination of TePixD at 5−200 K derived an EPR signal with a separation of 85 G between the main peaks around $g = 2$, showing a typical Pake's pattern of magnetic dipole−dipole interaction between two nearby radicals. Longer illumination induced an EPR signal at $g = 2.0045$, which was assigned as a neutral flavosemiquinone FADH•. The FADH• formation occurred in parallel with a decrease in Pake's doublet. The Pake's doublet was not detected in a mutant TePixD protein in which a tyrosine residue was replaced with phenylalanine (Y8F protein). A pulsed ENDOR study suggested that the Pake's doublet had arisen from the interaction between a neutral flavosemiquinone radical and a neutral tyrosine radical, i.e., the FADH•-Y8• state. An EPR simulation of the Pake's doublet showed that the distance between FAD and Y8 is 2.2 Å shorter than that calculated from the X-ray crystallography structure in the dark-adapted state, suggesting the modification of the protein conformation in the photoinduced FADH•-Y8• state. The Pake's doublet signal was detected by 10 K illumination in the sample which was immediately frozen after 273 K illumination, corresponding to the red-shifted state F_{490}. On the other hand, the signal was not detected in the sample which was incubated for 10 min at 273 K in the dark after 273 K illumination, corresponding to the dark-adapted state D_{471}. In the sample annealed at 160 K for 10 min after 160 K illumination, corresponding to the partially red-shifted state J_{11}, the Pake's doublet signal was detected by the 10 K illumination. On the basis of these observations, we concluded that the interaction with the FADH•-Y8• state occurred after the second photoexcitation of the photoinduced red-shifted states in the photocycle of TePixD.

The BLUF[1] (blue light using FAD) domain is a newly discovered blue light-sensing photoreceptor protein (*1*). Four groups of the BLUF domain are known at present: PixD (SyPixD in *Synechocystis* Pcc6803 or TePixD in *Thermosynechococcus elongatus*), AppA and BlrB in *Rhodobacter sphaeroides* (*1*−*3*), PAC in *Euglena gracilis* (*4*), and YcgF in *Escherichia coli* (*5*). PixD regulates pili-dependent cell motility (*6*). AppA controls the expression of the photosynthesis gene (*2*). PAC controls the photophobic movement of cells (*4*).

The BLUF domain protein shows a reversible 10−20 nm red shift of the flavin absorption bands upon light excitation at room temperature (*2, 3, 6*−*9*). The red-shifted form (signaling state) decays back to the dark-adapted state within 10−30 min. The structures of TePixD, SyPixD, AppA, and BlrB were determined by X-ray crystallography and NMR spectroscopy (*3, 10*−*14*). Figure 1 shows the crystal structure of the flavin-binding site of TePixD (*12*). The flavin isoalloxazine ring has been assumed to make hydrogen bondings with surrounding residues, Gln50, Asn31, Asn32, and Arg65 (the numbers are from TePixD structure). The Gln50 and Asn32 residues are well conserved in the BLUF domain.

FTIR and Raman studies have shown that the vibration of the C_4═O group in flavin is weakened, suggesting the stronger hydrogen bonding in the red-shifted form (*7, 15*−*22*). It was proposed that Gln50 also forms a hydrogen bond with N_5 (or additionally O_4) of flavin in the dark and alters it in the photoreaction because a mutant protein, which has Ala in place of Gln50 (Q50A), did not achieve the red-shifted form (*23*). The red-shifted final signaling form and the dark-adapted state of TePixD were named F_{490} and D_{471}, respectively, according to the wavelength of the red-shifted peak of flavin (*8*). Illumination at 5 K induced a smaller 5 nm red shift, designated as an I_5 intermediate form (*8*). The I_5 was converted to the 11 nm red-shifted form, designated as

[†] This work was supported by the JGC-S Scholarship Foundation (for H.M.), by a Research Fellowship for Young Scientist (18-645) (for Y.F.), and by Grant-in-Aid 20370018 for Scientific Research from the Ministry of Education, Culture, Sports, and Technology (for M.I.).

* Corresponding author. Phone: +81-52-789-2883. Fax:+81-52-789-2883. E-mail: mino@bio.phys.nagoya-u.ac.jp.

[‡] Nagoya University.

[§] University of Tokyo.

[||] Osaka Prefecture University.

[1] Abbreviations: BLUF, sensor of blue light using FAD; FAD, flavin adenine dinucleotide; ESE, electron spin echo; ENDOR, electron−nuclear double resonance; CW, continuous wave; WT, wild type.

10.1021/bi8010187 CCC: $40.75
Published on Web 10/31/2008

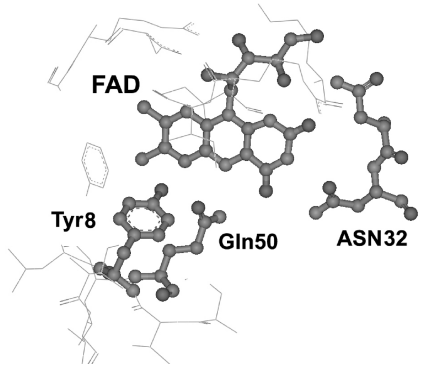

FIGURE 1: Local structure of FAD and surroundings of TePixD (PDB entry 1X0P, chain A) (*12*).

J_{11}, and then to F_{490} by further warming in the dark to 77 K and to above 260 K (*24*).

The molecular structure of TePixD suggests that Tyr8 interacts with flavin through a FAD-Gln50-Tyr8 hydrogen-bond network (*12*), where Tyr8 is a hydrogen-bond donor to the Gln50 in both the dark and light states (*25*). The replacement of tyrosine to phenylalanine (Y8F in TePixD and SyPixD, Y21F in AppA, and Y472F in PACR-F2) abolished the photoconversion activities at physiological temperatures (*16, 26*−*30*).

An ultrafast spectroscopy study of BLUF proteins detected the formation of the red-shifted form within 100 ps after the laser excitation, in parallel with the decay of the singlet excited state at room temperature (*31, 32*). Gauden et al. observed a FAD anion radical ($FAD^{\bullet -}$) and a subsequently formed neutral radical ($FADH^{\bullet}$) in SyPixD using transient absorption measurements (*31*). They proposed that the oxidation of the nearby tyrosine residue and subsequent formation of a $FADH^{\bullet}$-$Y^{\bullet}$ radical pair are essential for the photochemistry of a BLUF protein.

In this paper, we studied the radical states in the photoreaction of the BLUF protein by EPR measurements. We detected a light-induced EPR signal at the $g = 2$ region induced by the illumination of TePixD. Its spectral feature, composed of two inner and outer lines, can be assigned to the dipole interaction between the $FADH^{\bullet}$ radical and the $Y8^{\bullet}$ radical. On the basis of the analysis, we discussed the reaction mechanism of the radical formation and protein conformation change.

MATERIALS AND METHODS

Cloning, Expression, and Purification. The coding region of TePixD of *T. elongatus* was amplified from the genomic DNA by PCR with primers (5′-ACATATGGGACTACATCGCCTG-3′ and 5′-CAGATCTAGGATCCTTGACTCA-3′). PCR was performed with Pfu DNA polymerase (Stratagene), and the PCR products were cloned into *Srf*I-digested pPCR-Script (Stratagene). Site-directed mutagenesis of this His-TePixD was performed using the PCR-based QuickChange site-directed mutagenesis kit (Stratagene) as described elsewhere (*12, 26*). The sequenced DNAs were excised with *Nde*I and *Bgl*II and then inserted into pET28a (Novagen) to allow expression with an N-terminal $(His)_6$ tag. Plasmids carrying the desired amino acid substitutions were confirmed by nucleotide sequencing. Tagged proteins were expressed in *E. coli* BL21(DE3) pLysS with these recombinant plasmids in the presence of 20 μg/mL kanamycin for 18 h at 37 °C. Cells were harvested, frozen at −80 °C, thawed at 4 °C, and then resuspended in a 20 mM HEPES−NaOH (pH 7.5) buffer containing 1 M NaCl. After being disrupted by sonication, samples were centrifuged at 48000*g* for 1 h at 4 °C. His-tagged fusion proteins were purified from the supernatants by nickel affinity column chromatography (HiTrap Chelating HP; Amersham Biosciences, Piscataway, NJ). A sample was loaded on a column, washed, and then eluted with a 20 mM HEPES−NaOH (pH 7.5) buffer containing 1 M NaCl with 500 mM imidazole. The sample concentration was 250−750 μM for CW EPR, 2 mM for ESE measurements, and 100 μM for the calculation of the spin numbers.

CW EPR measurements were performed using a Bruker ESP-300E EPR spectrometer with a gas flow temperature control system (CF935; Oxford Instruments, Oxford, GB). A standard resonator (ER4102) was used. The TEMPO radical was used for the determination of the spin quantity as a standard sample. ESE experiments were performed on a pulsed EPR spectrometer, ESP-380 (Bruker), using a two-pulse (primary) ESE sequence. The spectrometer was equipped with a cylindrical dielectric cavity (ER4117DHQ-H; Bruker) and a gas flow temperature control system (CF935; Oxford Instruments). The measurement temperature was 30 K, and microwave (mw) pulses of 16 and 24 ns duration were used for $\pi/2-\pi$ pulses. The field-sweep ESE spectra were measured at the time interval τ of 200 ns between the mw pulses. In pulsed ENDOR measurements, the mw and radiofrequency (rf) pulse sequences introduced by Davies (*33*) were used. The rf pulse was amplified by a 500 W amplifier (ENI 500A). The durations of the mw pulses were 96, 48, and 96 ns. The separation between the first and second mw pulses was 20 μs. The separation between the second and third mw pulses was 200 ns, and the duration of the rf pulse applied between the first and second mw pulses was 6−10 μs. Samples were illuminated with a 408 nm diode laser (ITC 510; THORLABS) through glass fiber of 1 mm diameter.

The spin density distribution was calculated using the Gaussian03 program (*34*). The upbepbe/6-311 g(d) basis set was used (*35*−*38*).

RESULTS

Figure 2 shows the EPR spectra of the wild-type (WT) TePixD illuminated for (A) 0 min, (B) 3 min, (C) 28 min, and (D) 290 min at 150 K. No EPR signal was detected in the region of $g = 2$ in the dark state of WT TePixD (trace A). Short illumination derived a symmetrical EPR signal centered at around $g = 2$ (trace B) composed of four peaks, i.e., two large inner peaks with a separation of 86 G and two outer peaks with a separation of approximately 170 G. The EPR line shape was easily assigned as the Pake's doublet (*39*). A Pake's doublet, composed with two inner peaks and two outer peaks, arises from a spin−spin dipole interaction. Two inner peaks show the dipole vector perpendicular to the external field, and two outer peaks with the twice separation of the inner peaks show the dipole vector parallel to the external field (*39*). Further illumination induced the featureless EPR signal with a peak-to-peak separation of 19 G centered at $g = 2.0045$, alternated with the Pake's doublet

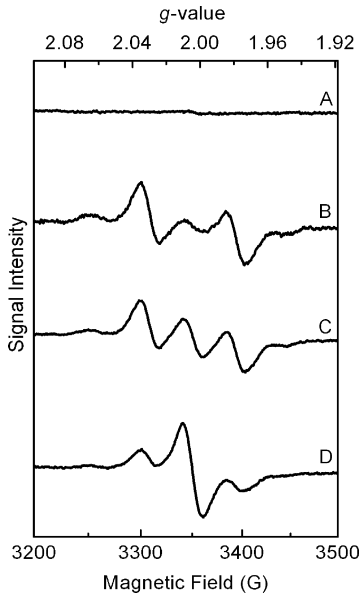

FIGURE 2: EPR spectra of TePixD measured after illumination for (A) 0 min, (B) 3 min, (C) 28 min, and (D) 290 min at 150 K. Experimental conditions: microwave power, 1 mW; microwave frequency, 9.40 GHz; modulation amplitude, 10 G; temperature, 150 K.

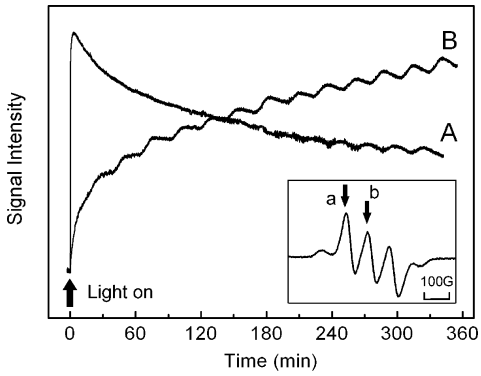

FIGURE 3: Time course of accumulations of EPR signals in WT-TePixD during illumination. Illumination was started at 0 min. Traces A and B were measured at the field positions indicated by arrows a and b in the inset, respectively. Experimental conditions are the same as in Figure 2.

(traces C and D). We assigned the featureless signal as a flavin neutral radical, in agreement with reported EPR properties (*40*).

Figure 3 shows the time courses of the magnitudes of the light-induced EPR signals of (A) the initial Pake's doublet signal and (B) the FADH• radical during illumination at 150 K. Traces A and B were observed at the low-field peak of the Pake's doublet (label a, inset) and the central peak of the FADH• radical (label b, inset). The modulation on the lines was caused by instability of the temperature. The doublet maximally accumulated with 1−2 min illumination and decayed gradually with a range of 6 h under illumination at 150 K, while the FADH• radical gradually accumulated in the range of 6 h during illumination at 150 K. Above 200 K, neither the FADH• nor the Pake's doublet signals were accumulated by fast decay (data not shown).

Figure 4 shows the time course of the decays of (A) the Pake's doublet signal and (B) the FADH• radicals measured in the dark after illumination at 150 K. The signals were observed at the field positions of Figure 3. The doublet signal

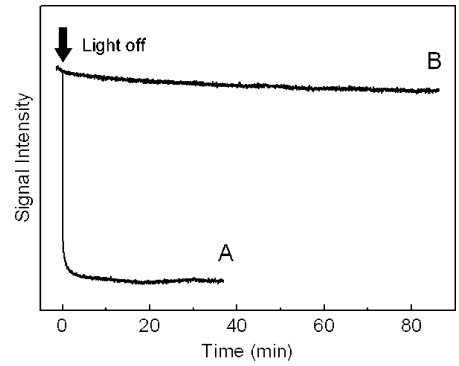

FIGURE 4: Dark decay time courses of EPR signals in TePixD. The signal intensities were measured at the field positions indicated by (A) arrow a, inset in Figure 3, and (B) arrow b, inset in Figure 3. Experimental conditions are the same as in Figure 2.

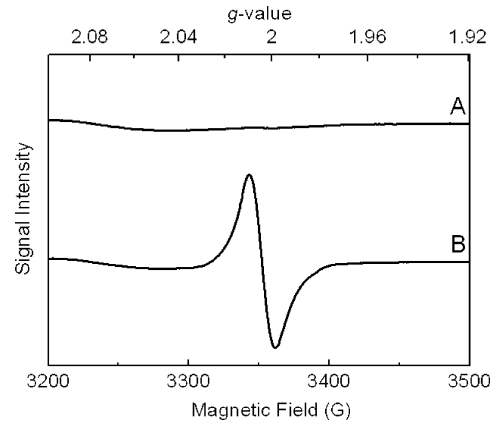

FIGURE 5: Light-induced EPR spectra in the Y8F mutant protein. The dark-adapted Y8F mutant protein was illuminated for (A) 0 min and (B) 20 min at 150 K. Experimental conditions are the same as in Figure 2.

decayed with 2 s, while the FADH• signal decayed little in the range of 90 min.

We calculated the spin quantities of both radicals. A diluted sample was used for ensuring full photoexcitation. The amount of the doublet signal was calculated from the spectrum obtained after 2 min illumination at 150 K. The amount of the FADH• signal was obtained from the spectrum after 1 h illumination, when almost all of the doublet signal was lost (data not shown). The obtained intensity ratio of the Pake's doublet signal and the FADH• radical was 1.6. The magnitude of spin S is generally expressed as $S = [S(S + 1)]^{1/2}$. As the doublet signal and the FADH• radical were described as $\boldsymbol{S} = 1$ and $\boldsymbol{S} = {}^1/_2$, respectively, the ratio of 1.6 for the amounts of the Pake's doublet signal and the FAD signal coincide. The amount of each radical was also estimated to be 70% of the total number of FAD.

Figure 5 shows the EPR spectra of the Y8F mutant TePixD (A) in the dark and (B) in the illuminated state for 20 min at 150 K. A light-induced EPR signal was detected with the peak-to-peak width of 19 G at $g = 2.0045$, which was identical with the FADH• radical detected in WT TePixD. On the other hand, the doublet signal observed in WT TePixD was not detected in the Y8F mutant. The results show that Tyr8 is essential for the formation of the Pake's doublet signal.

Figure 6 shows the field swept ESE spectra of (A) the doublet signal and (B) the FADH• radical. Trace A was obtained by illuminating for 3 min in WT TePixD at 150 K,

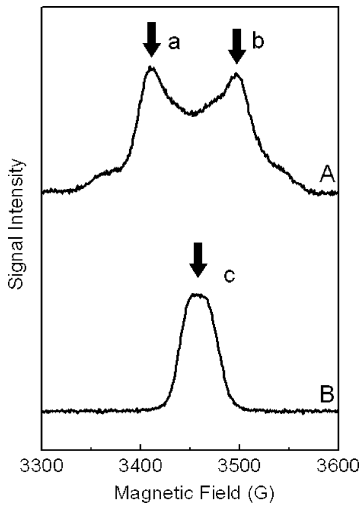

FIGURE 6: Primary ESE field-swept spectra of (A) wild-type and (B) Y8F mutant TePixD proteins measured at $\tau = 200$ ns. The dark-adapted proteins were illuminated for 3 min at 100 K. Experimental conditions: microwave frequency, 9.67 GHz; duration of the microwave pulses, 16 and 24 ns; repetition rate, 0.5 kHz; temperature, 30 K.

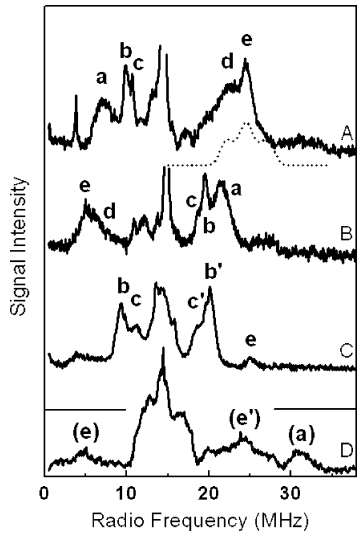

FIGURE 7: Davies ENDOR spectra of the (A, B) Pake's doublet signal and (C) FADH• signal. The signals (A, B, and C) were measured at the field positions indicated by arrows a, b, and c in Figure 6, respectively. (D) Tyrosine neutral radical Y_Z• (pH 7.5) observed in plant photosystem II (*42*). A dotted line in (A) shows a simulated spectrum (see text). Experimental conditions: microwave frequency, 9.67 GHz; duration of the microwave pulses, 96, 48, and 96 ns; interval between the first and second pulses, 20 μs; duration of RF, 6–10 μs; interval between the second and third pulses, 400 ns; temperature, 30 K.

and trace B was obtained by illuminating for 60 min in the Y8F mutant TePixD at 150 K. The obtained ESE spectra are equivalent to those obtained by the CW EPR measurement.

Figure 7 shows the Davies ENDOR spectra of (A, B) the Pake's doublet signal in WT and (C) the FADH• radical in the Y8F mutant. Traces A and B were obtained at the low-field peak (label a in Figure 6) and the high-field peak (label b in Figure 6) in the Pake's doublet, respectively. Trace C was obtained at the peak (label c in Figure 6) in the FADH• signal. Traces A and B show asymmetric line shapes centered on the resonant frequency of free proton ν_n around 15 MHz, ascribed to a typical ENDOR pattern of the $S = 1$ spin system (*41*). Scheme 1 shows the ENDOR patterns of the

Scheme 1: (A) Spin Energy Levels of the $S = 1$ and $I = {}^1/_2$ System Showing (a) Positive $A(+)$ and (b) Negative $A(-)$ Hyperfine Splitting[a] and (B) ENDOR Patterns Corresponding to the Transitions (a) from $m_s = 0$ to $m_s = 1$ and (b) from $m_s = -1$ to $m_s = 0$

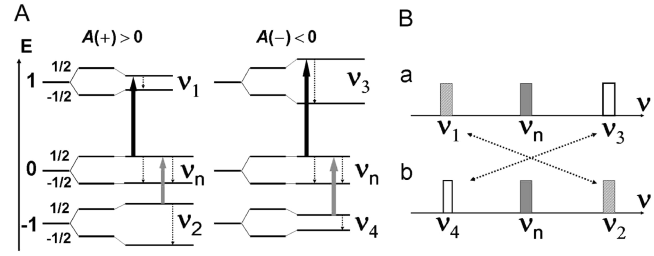

[a] In (A), black and gray arrows show the transitions between $m_s = 0$ and $m_s = 1$ and those between $m_s = -1$ and $m_s = 0$, respectively. Dotted arrows show the ENDOR transitions.

Scheme 2: Molecular Structure of (A) Neutral Flavinosemiquinone (FADH) and (B) Tyrosine

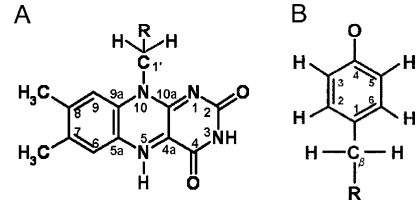

spin system $S = 1$ and $I = {}^1/_2$, with a hyperfine interaction defined as $A \cdot S$. In the case of the positive hyperfine constant $A(+)$, two NMR transitions of free proton frequency ν_n and lower frequency ν_1 can be detected in the EPR transition at the low-field side. Two NMR transitions of free proton frequency ν_n and higher frequency ν_2 can be detected in the EPR transition at the high-field side. In the case of negative hyperfine constant $A(-)$, these features are opposite. Therefore, we can evaluate the sign of the hyperfine constants from the $S = 1$ ENDOR spectrum.

Traces A and B in Figure 7 show five ENDOR peaks labeled a−e. Trace D is the ENDOR spectrum of the tyrosine neutral radical Y_Z detected at pH 7.5 in photosystem II (*42*). Peak e is generally detected within tyrosine neutral radicals (*43, 44*), ascribed to the $C_{3,5}$ α-protons in a tyrosine neutral radical (Scheme 2B), assigned to the negative sign of hyperfine. Therefore, we can assign peaks a−c as positive and peaks d and e as negative for hyperfine constants. Trace C shows the symmetrical ENDOR pattern against ν_n, ascribed to the typical $S = {}^1/_2$ spin system. Three ENDOR peaks labeled b, c, and e in trace c were assigned as a neutral FADH• radical (*40, 45*).

To investigate the property of the intermediate state, different samples were prepared. The PRE1 sample was frozen to 77 K immediately after 273 K illumination for 1 min. The DARK1 sample was incubated for 10 min at 273 K and subsequently frozen to 77 K after 273 K illumination for 1 min. The PRE1 sample was supposed to be populated in the red-shifted state F_{490}. The DARK1 sample was supposed to be populated in the ground state D_{471}. Figure 8 shows the EPR spectra of the light-induced Pake's doublet signals. Panel A shows the time course of the Pake's doublet signal in (a) the PRE1 sample and (b) the PRE2 sample during illumination. The signals were observed at the field

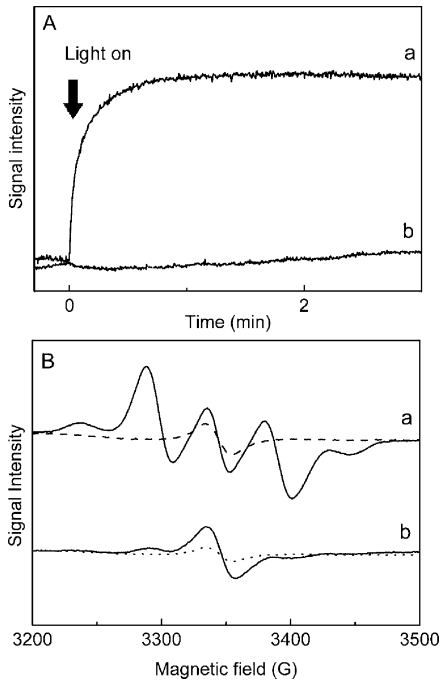

FIGURE 8: (A) Time courses of the formation of (B) field-swept EPR spectra the Pake's doublet signal in the (a) PRE1 and (b) DARK1 samples. The signals were measured at the field positions indicated by arrow a (inset) in Figure 3. Experimental conditions are the same as in Figure 2 except for the temperature, 10 K.

position of the inner low peak (label a in Figure 3). Panel B shows the field-swept EPR spectra of the (a) PRE1 and (b) DARK1 samples. The dotted lines show the spectra before the illumination of the PRE1 and DARK1 samples. The Pake's doublet signal was observed in the PRE1 sample, populated in the F_{490} state, but not in the DARK1 sample, populated in the D_{471} state.

Furthermore, two samples, DARK2 and PRE2, were examined. The DARK2 sample was incubated at 273 K for 10 min in the dark after 160 K illumination for 10 min. In the DARK2 condition, the sample was supposed to be populated in the ground state, D_{471}. The PRE2 sample was incubated in the dark at 160 K for 10 min after 160 K illumination for 10 min. In the PRE2 condition, the sample was supposed to be populated in the J_{11} state. Figure 9 shows the time course of the light-induced formations of the Pake's doublet signals in PRE2 (A, C, and E) and DARK2 (B, D, and F) samples in WT TePixD at (A, B) 100 K, (C, D) 40 K, and (E, F) 10 K, respectively. The signals were observed at the field position of the inner low peak (label a in Figure 3). The kinetics and yield of the doublet signal were identical at 100 K in both samples, DARK2 and PRE2 (traces A and B). Below 80−100 K, the signal intensity in the DARK2 sample gradually decreased (trace D). At 10 K, no Pake's doublet signal was detected in the DARK2 sample (trace F), in contrast with the PRE2 sample (trace E). The difference in the DARK2 and PRE2 samples can be ascribed to the differences in the initial intermediate states in the photocycle (*8, 24*).

DISCUSSION

Formation of Light-Induced Radicals. In this paper, we detected two types of light-induced EPR signals in WT TePixD. CW and ESE field-swept EPR showed that one signal arises from the "Pake's doublet" and the other signal

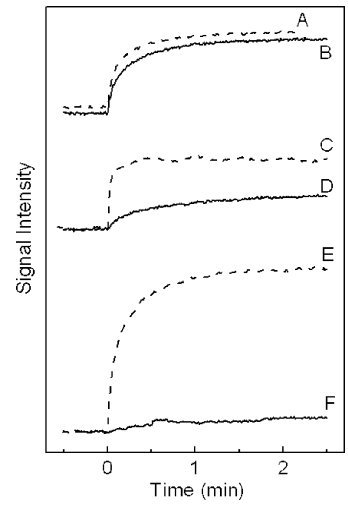

FIGURE 9: Time courses of the formation of the Pake's doublet signal in the (bold) DARK2 and (dotted) PRE2 samples. The signals were measured at the field positions indicated by arrow a (inset) in Figure 3. The DARK2 sample was incubated at 273 K for 10 min in the dark after 160 K illumination for 10 min. The PRE2 sample was initially illuminated at 160 K and then incubated in the dark at 160 K for 10 min. Experimental conditions are the same as in Figure 2 except for the temperature: (A, B) 100 K, (C, D) 40 K, and (E, F) 10 K.

arises from the neutral $FADH^{\bullet}$ radical (*40, 45*). In the Y8F mutant, only the $FADH^{\bullet}$ neutral radical was accumulated. The results showed that the Tyr8 residue is essential for the formation of the Pake's doublet signal. Davies ENDOR showed the involvement of the tyrosine neutral radical and the $FADH^{\bullet}$ neutral radical in the doublet signal. The feature of the Pake's doublet is similar to that reported in proteins arising from the closely located neutral radicals, including the tyrosine residue (*43, 46, 47*).

The Pake's doublet signal was induced immediately after illumination. On the other hand, the photoaccumulation of the $FADH^{\bullet}$ was very slow, on the order of hours. The FAD radical in TePixD has been reported by absorption measurement, though it was assigned as an anion radical (*24*). The $FADH^{\bullet}$ radical was observed in both WT and Y8F mutant proteins, indicating the formation of the $FADH^{\bullet}$ radical does not require the Y8 residue. The $FADH^{\bullet}$ radical may be caused by a minor pathway after many turnovers of the photoexcitation of FAD(H) under illumination. During illumination at 150 K, the Pake's doublet shows monophasic decay, and the $FADH^{\bullet}$ radical shows a biphasic increase. The inconsistency of the decay kinetics of the Pake's doublet and the increase of the $FADH^{\bullet}$ radical indicate that the formations of the Pake's doublet and the $FADH^{\bullet}$ radical are independent. On the other hand, the maximum quantities of both radicals were 70% of all flavin molecules in the sample, indicating that most of the centers forming the doublet signal in the sample were converted to the $FADH^{\bullet}$ radical in WT during long illumination.

Simulation of the Pake's Doublet Signal Based on the Crystal Structure. Pake's doublet is expressed as the electron−electron magnetic dipole interaction. Assuming a point-dipole approximation, the distance defined as the separation between inner peaks is described by the equation:

$$\Delta\nu = g_e\beta g_n\beta_n/r^3 \quad (1)$$

Table 1: Spin Density Distributions on the Tyrosine Neutral Radical and the FADH• Radical[a]

FADH• radical				neutral tyrosine radical	
atom	spin density	atom	spin density	atom	spin density
N(1)	0.07	C(5a)	0.01	C(1)	0.35
C(2)	−0.01	C(6)	0.02	C(2)	−0.10
O(2)	0.05	C(7)	0.00	C(3)	0.26
N(3)	0.00	C(8)	0.05	C(4)	−0.04
C(4)	−0.01	C(9)	−0.02	O(4)	0.36
O(4)	0.12	C(9a)	0.06	C(5)	0.25
C(4a)	0.42	N(10)	0.09	C(6)	−0.10
N(5)	0.17	C(10a)	−0.05		

[a] The numberings of the atoms are illustrated in Scheme 2.

where r is the distance between radicals, g_e and g_n are g-factors for electrons and nuclei, respectively, and β and β_n are Bohr magnetrons for electrons and nuclei, respectively. The separation between the inner peaks in the doublet signal is 86 G, which gives the distance of 6.9 Å. The structure of TePixD shows that Tyr8 is the only candidate for forming a stable radical around the FAD molecule. On the other hand, the electron spins actually delocalized on the molecules. To simulate the EPR signal more precisely, the spin density distributions on the neutral tyrosine radical and FADH neutral radical were calculated using Gaussian03. The obtained spin densities are listed in Table 1. The dipole interaction was described by the equation:

$$\Delta\nu = g\beta g_n\beta_n\Sigma_{i,j}(1 - 3\cos^2\theta_{i,j})\rho_i\rho_j/r_{i,j}^3 \qquad (2)$$

where ρ_i and ρ_j are the spin densities on the ith atom on one radical and the jth atom on the other radical, respectively, and $r_{i,j}$ and $\theta_{i,j}$ are the distance and angle between the external field vector and the vector connecting ρ_i and ρ_j, respectively. For the simulation of the Pake's doublet signal, we used the coordinates of Tyr8 and FAD based on the crystal structure and spin density distribution (Table 1). Trace C in Figure 10 is the simulated spectrum. The obtained hyperfine separations were 36 G, which is 0.4 times smaller than those in the experimental spectrum (traces A and B, Figure 10). The result indicates that the distance between the Tyr8 and FAD radicals is smaller than those in the crystal structure. To simulate the experimental spectrum, the distance between radicals is shortened on the line between O_4 on Tyr8 and C_{4a} carbon on FAD. Trace D shows the simulated spectrum, where the coordinates of Tyr8 are brought 2.2 Å closer toward the FAD molecule.

Assignment of ENDOR Signals. The ENDOR spectrum of the tyrosine neutral radical is mainly composed of large hyperfine interactions of two equivalent $C_{3,5}$ α-protons and β-methylene protons. The hyperfine constant for the $C_{3,5}$ α-proton is negative, and that for the β-methylene proton is positive. The ENDOR spectrum of the FADH• radical is mainly composed of hyperfine interactions of the C_1'-H, $C_{8\alpha}$-H, and N_5-H protons. The hyperfine constants for the C_1'-H and $C_{8\alpha}$-H protons are positive, and that for the N_5-H proton is negative. We detected five ENDOR peaks in the Pake's doublet signal, labeled as a−e in Figure 7. The obtained spectral patterns at the low- and high-field positions were opposite against the free proton frequency ν_H. The result is in consistence with the signal with the $\mathbf{S} = 1$ spin state. Peaks a−c are assigned a positive sign, and peaks d and e are assigned a negative sign. By comparison with the ENDOR pattern and spin density distributions on tyrosine and FAD, the larger peak e can be ascribed to the $C_{3,5}$ α-protons in the tyrosine neutral radical, although the relatively small peak of the N_5-H proton might overlap. Labels b and c can be assigned to the C_1'-H proton and the $C_{8\alpha}$-H proton in the FADH• radical, respectively. Peak a was assigned as the β-methylene protons in Tyr8. The hyperfine constant A_β of β-methylene is determined by the spin density ρ_1 on the ring carbon C_1 and the dihedral angle θ between the plane formed by C_1, C_β, and H_β and the plane determined by the p-orbital on C_1 and the C_1−C_β bond:

$$A_\beta \approx \rho_1 B\cos^2\theta \qquad (3)$$

where B is a constant of the order of 162 MHz (*48*). Based on the MO calculation, the value of ρ_1 is estimated as 0.35 in a tyrosine neutral radical (Table 1). Assuming that peak a arises from β-methylene protons, the dihedral angle is estimated as $\theta = 59.5°$, indicating that the signals of two β-methylene protons overlap on the position of label a as a large amplitude. The results are the same as those in the crystal structure, where the dihedral angles for both β-methylene protons on Tyr8 are approximately 60° (*12*).

In order to identify peak d, we simulated the ENDOR spectra in more detail. The ENDOR spectra of the Pake's doublet signal (traces A and B, Figure 7) were measured at the inner peak positions (arrays a and b, Figure 5), indicating that the magnetic dipole vector between Tyr8 and FAD is 90° or 35° to the external field (*39*). We assumed the angle to be 90° as the major contribution. The hyperfine tensor components for the $C_{3,5}$ α-proton were assumed as $A_X = -26.5$ MHz, $A_Y = -20.3$ MHz, and $A_Z = -9.6$ MHz (*42, 44*). The direction of the dipole vector was assumed to be on the line between the ring center on Tyr8 and C_{4a} carbon on FAD. The dotted line in Figure 7 shows the simulated ENDOR spectrum for $C_{3,5}$ α-protons, where the coordinates of Tyr8 obtained by the crystal structure were rotated at the angle of

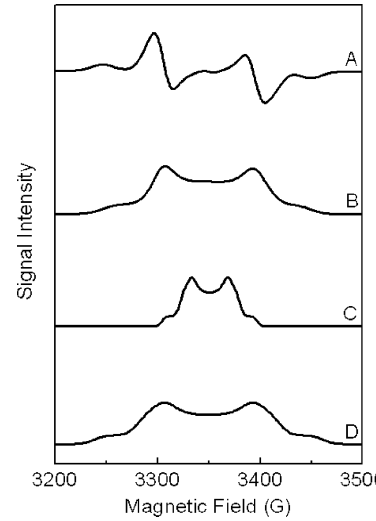

FIGURE 10: EPR spectra of (A) the experimental derivative-type spectrum and (B) the absorption-type spectrum obtained by integrating the spectrum in (A). (C, D) Simulated absorption-type spectra. For the calculation of trace C, the spin density distributions listed in Table 1 were used. The atomic coordinates of flavin and Tyr8 were obtained from the PDB database (1X0P, chain A) (*12*). For the calculation of trace D, the atomic coordinates of Tyr8 were moved to achieve a 2.2 Å closer distance toward the FAD molecule.

Table 2: Hyperfine Coupling Constants and Assignments of the ENDOR Signals (MHz)

label	a	b	c	d	e
Pake's doublet signal	7.3	4.5	3.9	−7.9	−10.1
FADH• (in Y8F)		10.8	7.4		−21.0
FADH•[a]			8.4		−18.4
FADH•[b]		9.0	7.5		−23.0
tyrosine Z[c]	33.6				−20.3
assignment	Tyr-C-H_β	FADH•-C(1′)H	FADH•-C(8α)H_3	Tyr-C(3,5) H	Tyr-C(3,5) H, FADH•-N(5)-H

[a] Reference *40*. [b] Reference *45*. [c] Reference *42*. Note that the hyperfine constants for the Pake's doublet were estimated as $S = 1$.

35° on the ring plane. The results show that peak d is explained by part of the partially oriented component of the $C_{3,5}$ α-protons on Tyr8. It is difficult to determine the accurate direction of the dipole vector between Tyr8 and FAD because the electron spin was delocalized on each radical. Therefore, it is unclear whether or not the molecular orientation of Tyr8 relative to the FAD radical is modified. However, no large modification of the molecular orientation seems to occur in the crystal structure because it is possible to explain the ENDOR spectrum without making a large change in the molecular orientation. In fact, the dihedral angles of the β-methylene protons in the Tyr8 radical were almost the same as those in the crystal structure (dark state). The assignments of the hyperfine constants are summarized in Table 2.

Temperature Dependence of the Formation of Radicals. We have measured the temperature dependence of the formation of the Pake's doublet. After the sample was incubated for 10 min at 273 K in the dark (DARK1 sample) after 273 K illumination, no Pake's doublet signal was detected at 10 K illumination. On the other hand, the Pake's doublet signal was detected at 10 K illumination in the sample (PRE1) which was immediately frozen after 273 K illumination. The PRE1 and DARK1 samples were assumed to be populated in F_{490} and D_{471} states, respectively. After the sample was incubated for 10 min at 273 K in the dark (DARK2 sample), no Pake's doublet signal was detected at 10 K illumination. On the other hand, after the sample was initially illuminated for 10 min at 160 K and subsequently incubated in the dark at 160 K for 10 min (PRE2 sample), the Pake's doublet signal was detected by the 10 K illumination. Two kinds of samples (DARK2 and PRE2) show different temperature dependence of the formation of the doublet signal below 80−100 K illumination. Fukushima et al. reported the occurrence of temperature-dependent changes in the accumulation of the intermediate states in the photocycle in TePixD. Above 50−80 K illumination, the ground state D_{471} is excited to the red-shift states J_{11} under illumination (*8*). Below 50−80 K illumination, the photocycle is trapped in the intermediate states I_5. These temperature dependences are coincident with the formation of the Pake's doublet signal in the DARK2 sample. The PRE2 sample could be initially populated in the J_{11} states. Therefore, we conclude that the Pake's doublet signal is formed by the photoexcitation of the red-shift states, both F_{490} and J_{11}, in the photocycle (Scheme 3). Recently, Toh et al. have proposed a second photoreaction after forming the red-shifted state in the AppA protein (*49*).

Scheme 3: Schematic Model of the Photocycle of TePixD Based on the Temperature Dependence of the Formation of the Pake's Doublet

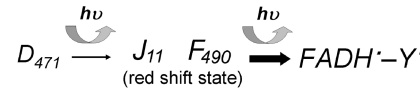

Driving Force in the Formation of FADH•-Y8• Radicals. The result of the EPR simulation for the Pake's doublet showed that the distance between the flavin molecule and the Tyr8 molecule on the FADH•-Y8• state is shorter at a distance of 2.2 Å against the crystal structure in the dark state (*12*), indicating the conformational modifications around Y8. The stability of the two closely located radicals can be explained as the neutral radicals with less electrostatic disturbance (*43, 47*). It is notable that all residues around Tyr8, except for Gln50, are hydrophilic. It has been proposed that the conformational modification of Gln50 derives the red-shift state (*13, 32*). If the interaction between Tyr8 and Gln50 is weakened by the modification of Gln50 as the steric hindrance, Tyr8 may be pressed by the surrounded hydrophilic environment, resulting in a reduced distance between Tyr8 and FAD. When the interdistance of the radicals is shortened on the line between the ring center on Tyr8 and C_{4a} carbon on FAD (trace D, Figure 10), the distance of O in Tyr8 and N_5 in FAD is 2.3 Å shorter. The structural modification around Y8 may control the stability of the FADH•-Y8•. The close proximity suggests the possibility of hydrogen bonding between Tyr8 and FAD.

Role of the Coupling of FADH• and Y8•. Gauden et al. observed a FAD anion radical ($FAD^{\bullet -}$) and a subsequently formed neutral radical (FADH•) in SyPixD using transient absorption measurements (*31*). They proposed that the radical pair mechanism including proton-coupled electron transfer is essential for the fast reaction mechanisms in BLUF (*31*), where the radical pair is assumed as the transient intermediate state upon the photoexcitation of the dark-adapted state before the formation of the red-shifted final signaling state at physiological temperature. Until now, no tyrosine radical has been detected by transient absorption spectroscopy at any temperature. In this paper, we showed the FADH•-Y8• state could be induced by the photoexcitation of the red-shifted states, where the structure nearby the C_4═O group would be changed. The proteins are illuminated even on the red-shifted state in the physiological condition. Therefore, the formation of the FADH•-Y8• pair on the red-shifted state might play some role in signal transferring on the TePixD.

REFERENCES

1. Gomelsky, M., and Klug, G. (2002) BLUF: a novel FAD-binding domain involved in sensory transduction in microorganisms. *Trends Biochem. Sci. 27*, 497–500.
2. Masuda, S., and Bauer, C. E. (2002) AppA is a blue light photoreceptor that antirepresses photosynthesis gene expression in *Rhodobacter sphaeroides*. *Cell 110*, 613–623.
3. Jung, A., Domratcheva, T., Tarutina, M., Wu, Q., Ko, W. H., Shoeman, R. L., Gomelsky, M., Gardner, K. H., and Schlichting, L. (2005) Structure of a bacterial BLUF photoreceptor: Insights into blue light-mediated signal transduction. *Proc. Natl. Acad. Sci. U.S.A. 102*, 12350–12355.

4. Iseki, M., Matsunaga, S., Murakami, A., Ohno, K., Shiga, K., Yoshida, K., Sugai, M., Takahashi, T., Hori, T., and Watanabe, M. (2002) A blue-light-activated adenylyl cyclase mediates photoavoidance in *Euglena gracilis*. *Nature 415*, 1047–1051.
5. Rajagopal, S., Key, J. M., Purcell, E. B., Boerema, D. J., and Moffat, K. (2004) Purification and initial characterization of a putative blue light-regulated phosphodiesterase from *Escherichia coli*. *Photochem. Photobiol. 80*, 542–547.
6. Okajima, K., Yoshihara, S., Fukushima, Y., Geng, X. X., Katayama, M., Higashi, S., Watanabe, M., Sato, S., Tabata, S., Shibata, Y., Itoh, S., and Ikeuchi, M. (2005) Biochemical and functional characterization of BLUF-type flavin-binding proteins of two species of cyanobacteria. *J. Biochem. 137*, 741–750.
7. Laan, W., van der Horst, M. A., van Stokkum, I. H., and Hellingwerf, K. J. (2003) Initial characterization of the primary photochemistry of AppA, a blue-light-using flavin adenine dinucleotide-domain containing transcriptional antirepressor protein from *Rhodobacter sphaeroides*: A key role for reversible intramolecular proton transfer from the flavin adenine dinucleotide chromophore to a conserved tyrosine? *Photochem. Photobiol. 78*, 290–297.
8. Fukushima, Y., Okajima, K., Shibata, Y., Ikeuchi, M., and Itoh, S. (2005) Primary intermediate in the photocycle of a blue-light sensory blue-light FAD-protein, Tll0078, of *Thermosynechococcus elongatus* BP-1. *Biochemistry 44*, 5149–5158.
9. Zirak, P., Penzkofer, A., Schiereis, T., Hegemann, P., Jung, A., and Schlichting, I. (2006) Photodynamics of the small BLUF protein BlrB from *Rhodobacter sphaeroides*. *J. Photochem. Photobiol. B 83*, 180–194.
10. Jung, A., Reinstein, J., Domratcheva, T., Shoeman, R. L., and Schlichting, I. (2006) Crystal structures of the AppA BLUF domain photoreceptor provide insights into blue light-mediated signal transduction. *J. Mol. Biol. 362*, 717–732.
11. Yuan, H., Anderson, S., Masuda, S., Dragnea, V., Moffat, K., and Bauer, C. (2006) Crystal structures of the *Synechocystis* photoreceptor Slr1694 reveal distinct structural states related to signaling. *Biochemistry 45*, 12687–12694.
12. Kita, A., Okajima, K., Morimoto, Y., Ikeuchi, M., and Miki, K. (2005) Structure of a cyanobacterial BLUF protein, Tll0078, containing a novel FAD-binding blue light sensor domain. *J. Mol. Biol. 349*, 1–9.
13. Anderson, S., Dragnea, V., Masuda, S., Ybe, J., Moffat, K., and Bauer, C. (2005) Structure of a novel photoreceptor, the BLUF domain of AppA from *Rhodobacter sphaeroides*. *Biochemistry 44*, 7998–8005.
14. Grinstead, J. S., Hsu, S. T. D., Laan, W., Bonvin, A. M. J. J., Hellingwerf, K. J., Boelens, R., and Kaptein, R. (2006) The solution structure of the AppA BLUF domain: Insight into the mechanism of light-induced signaling. *ChemBioChem 7*, 187–193.
15. Hasegawa, K., Masuda, S., and Ono, T. (2004) Structural intermediate in the photocycle of a BLUF (sensor of blue light using FAD) protein Slr1694 in a cyanobacterium *Synechocystis* sp. PCC6803. *Biochemistry 43*, 14979–14986.
16. Hasegawa, K., Masuda, S., and Ono, T. A. (2005) Spectroscopic analysis of the dark relaxation process of a photocycle in a sensor of blue light using FAD (BLUF) protein Slr1694 of the cyanobacterium *Synechocystis* sp. PCC6803. *Plant Cell Physiol. 46*, 136–146.
17. Hasegawa, K., Masuda, S., and Ono, T. (2006) Light induced structural changes of a full-length protein and its BLUF domain in YcgF(Blrp), a blue-light sensing protein that uses FAD (BLUF). *Biochemistry 45*, 3785–3793.
18. Masuda, S., Hasegawa, K., and Ono, T. (2005) Adenosine diphosphate moiety does not participate in structural changes for the signaling state in the sensor of blue-light using FAD domain of AppA. *FEBS Lett. 579*, 4329–4332.
19. Masuda, S., Hasegawa, K., and Ono, T. (2005) Light-induced structural changes of apoprotein and chromophore in the sensor of blue light using FAD (BLUF) domain of AppA for a signaling state. *Biochemistry 44*, 1215–1224.
20. Masuda, S., Hasegawa, K., and Ono, T. A. (2005) Tryptophan at position 104 is involved in transforming light signal into changes of beta-sheet structure for the signaling state in the BLUF domain of AppA. *Plant Cell Physiol. 46*, 1894–1901.
21. Unno, M., Masuda, S., Ono, T. A., and Yamauchi, S. (2006) Orientation of a key glutamine residue in the BLUF domain from AppA revealed by mutagenesis, spectroscopy, and quantum chemical calculations. *J. Am. Chem. Soc. 128*, 5638–5639.
22. Unno, M., Sano, R., Masuda, S., Ono, T. A., and Yamauchi, S. (2005) Light-induced structural changes in the active site of the BLUF domain in AppA by Raman spectroscopy. *J. Phys. Chem. B 109*, 12620–12626.
23. Grinstead, J. S., Avila-Perez, M., Hellingwerf, K. J., Boelens, R., and Kaptein, R. (2006) Light-induced flipping of a conserved glutamine sidechain and its orientation in the AppA BLUF domain. *J. Am. Chem. Soc. 128*, 15066–15067.
24. Fukushima, Y., Okajima, K., Ikeuchi, M., and Itoh, S. (2007) Two intermediate states I and J trapped at low temperature in the photocycles of two BLUF domain proteins of cyanobacteria Synechocystis sp. PCC6803 and *Thermosynechococcus elongatus* BP-1. *Photochem. Photobiol. 83*, 112–121.
25. Takahashi, R., Okajima, K., Suzuki, H., Nakamura, H., Ikeuchi, M., and Noguchi, T. (2007) FTIR study on the hydrogen bond structure of a key tyrosine residue in the flavin-binding blue light sensor TePixD from *Thermosynechococcus elongatus*. *Biochemistry 46*, 6459–6467.
26. Okajima, K., Fukushima, Y., Suzuki, H., Kita, A., Ochiai, Y., Katayama, M., Shibata, Y., Miki, K., Noguchi, T., Itoh, S., and Ikeuchi, M. (2006) Fate determination of the flavin photoreceptions in the cyanobacterial blue light receptor TePixD (T110078). *J. Mol. Biol. 363*, 10–18.
27. Ito, S., Murakami, A., Sato, K., Nishina, Y., Shiga, K., Takahashi, T., Higashi, S., Iseki, M., and Watanabe, M. (2005) Photocycle features of heterologously expressed and assembled eukaryotic flavin-binding BLUF domains of photoactivated adenylyl cyclase (PAC), a blue-light receptor in *Euglena gracilis*. *Photochem. Photobiol. Sci. 4*, 762–769.
28. Dragnia, V., Anderson, S., Masuda, S., Waegelle, M., Balascuta, S., Ybe, J., Dragnea, B., Moffat, K., and Bauer, C. (2005) Crystallographic and functional studies of the AppA blue-light receptor BLUF domain from *Rhodobacter sphaeroides*. *Abstr. Pap. Am. Chem. Soc. 230*, U2809–U2809.
29. Gauden, M., Grinstead, J. S., Laan, W., van Stokkum, H. M., Avila-Perez, M., Toh, K. C., Boelens, R., Kaptein, R., van Grondelle, R., Hellingwerf, K. J., and Kennis, J. T. M. (2007) On the role of aromatic side chains in the photoactivation of BLUF domains. *Biochemistry 46*, 7405–7415.
30. Kraft, B. J., Masuda, S., Kikuchi, J., Dragnea, V., Tollin, G., Zaleski, J. M., and Bauer, C. E. (2003) Spectroscopic and mutational analysis of the blue-light photoreceptor AppA: A novel photocycle involving flavin stacking with an aromatic amino acid. *Biochemistry 42*, 6726–6734.
31. Gauden, M., van Stokkum, I. H. M., Key, J. M., Luhrs, D. C., Van Grondelle, R., Hegemann, P., and Kennis, J. T. M. (2006) Hydrogen-bond switching through a radical pair mechanism in a flavin-binding photoreceptor. *Proc. Natl. Acad. Sci. U.S.A. 103*, 10895–10900.
32. Gauden, M., Yeremenko, S., Laan, W., van Stokkum, I. H. M., Ihalainen, J. A., van Grondelle, R., Hellingwerf, K. J., and Kennis, J. T. M. (2005) Photocycle of the flavin-binding photoreceptor AppA, a bacterial transcriptional antirepressor of photosynthesis genes. *Biochemistry 44*, 3653–3662.
33. Davies, E. R. (1974) New Pulse ENDOR Technique. *Phys. Lett. A 47*, 1–2.
34. Frisch, M. J., Trucks, G. W., Schlegel, H. B., Scuseria, G. E., Robb, M. A., Cheeseman, J. R., Montgomery, J. A., Jr., Vreven, T., Kudin, K. N., Burant, J. C., Millam, J. M., Iyengar, S. S., Tomasi, J., Barone, V., Mennucci, B., Cossi, M., Scalmani, G., Rega, N., Petersson, G. A., Nakatsuji, H., Hada, M., Ehara, M., Toyota, K., Fukuda, R., Hasegawa, J., Ishida, M., Nakajima, T., Honda, Y., Kitao, O., Nakai, H., Klene, M., Li, X., Knox, J. E., Hratchian, H. P., Cross, J. B., Bakken, V., Adamo, C., Jaramillo, J., Gomperts, R., Stratmann, R. E., Yazyev, O., Austin, A. J., Cammi, R., Pomelli, C., Ochterski, J. W., Ayala, P. Y., Morokuma, K., Voth, G. A., Salvador, P., Dannenberg, J. J., Zakrzewski, V. G., Dapprich, S., Daniels, A. D., Strain, M. C., Farkas, O., Malick, D. K., Rabuck, A. D., Raghavachari, K., Foresman, J. B., Ortiz, J. V., Cui, Q., Baboul, A. G., Clifford, S., Cioslowski, J., Stefanov, B. B., Liu, G., Liashenko, A., Piskorz, P., Komaromi, I., Martin, R. L., Fox, D. J., Keith, T., Al-Laham, M. A., Peng, C. Y., Nanayakkara, A., Challacombe, M., Gill, P. M. W., Johnson, B., Chen, W., Wong, M. W., Gonzalez, C., and Pople, J. A. (2004)Gaussian 03, revision C.02, Gaussian, Inc., Wallingford, CT.
35. Mclean, A. D., and Chandler, G. S. (1980) Contracted gaussian-basis sets for molecular calculations 0.1. 2nd row atoms, $Z=11-18$. *J. Chem. Phys. 72*, 5639–5648.

36. Krishnan, R., Binkley, J. S., Seeger, R., and Pople, J. A. (1980) Self-consistent molecular-orbital methods 0.20. Basis set for correlated wave-functions. *J. Chem. Phys. 72*, 650–654.
37. Perdew, J. P., Burke, K., and Ernzerhof, M. (1996) Generalized gradient approximation made simple. *Phys. Rev. Lett. 77*, 3865–3868.
38. Perdew, J. P., Burke, K., and Ernzerhof, M. (1997) Generalized gradient approximation made simple. *Phys. Rev. Lett. 78*, 1396–1396.
39. Pake, G. E., and Gutowsky, H. S. (1948) Nuclear relaxation in ice at−180°C. *Phys. Rev. 74*, 979–980.
40. Medina, M., and Cammack, R. (2007) ENDOR and related EMR methods applied to flavoprotein radicals. *Appl. Magn. Reson. 31*, 457–470.
41. Kurreck, H., Kirste, B., and Lubitz, W. (1988) in *Electron Nuclear Double Resonance Spectroscopy of Radicals in Solution*, pp 251−277, VCH Publishers, New York.
42. Mino, H., Astashkin, A. V., and Kawamori, A. (1997) An EPR and pulsed ENDOR study of the structure of tyrosine $Z^{\cdot}$ in Tris-treated photosystem II. *Spectrochim. Acta A 53*, 1465–1483.
43. Astashkin, A. V., Mino, H., Kawamori, A., and Ono, T. A. (1997) Pulsed EPR study of the S_3' signal in the Ca^{2+}-depleted photosystem II. *Chem. Phys. Lett. 272*, 506–516.
44. Bender, C. J., Sahlin, M., Babcock, G. T., Barry, B. A., Chandrashekar, T. K., Salowe, S. P., Stubbe, J., Lindstrom, B., Petersson, L., Ehrenberg, A., and Sjoberg, B. M. (1989) An ENDOR Study of the tyrosyl free-radical in ribonucleotide reductase from *Escherichia coli*. *J. Am. Chem. Soc. 111*, 8076–8083.
45. Kay, C. W. M., Feicht, R., Schulz, K., Sadewater, P., Sancar, A., Bacher, A., Mobius, K., Richter, G., and Weber, S. (1999) EPR, ENDOR, and TRIPLE resonance spectroscopy on the neutral flavin radical in DNA photolyase. *Biochemistry 38*, 16740–16748.
46. Mino, H., Kawamori, A., and Ono, T. (2000) Pulsed EPR studies of doublet signal and singlet-like signal in oriented Ca^{2+}-depleted PSII membranes: Location of the doublet signal center in PSII. *Biochemistry 39*, 11034–11040.
47. Mino, H., and Itoh, S. (2005) The origin of split EPR signals in the Ca^{2+}-depleted photosystem II. *Photosynth. Res. 84*, 333–337.
48. Fessenden, R. W., and Schuler, R. H. (1963) Electron spin resonance studies of transient alkyl radicals. *J. Chem. Phys. 39*, 2147–2195.
49. Toh, K. C., van Stokkum, I. H. M., Hendriks, J., Alexandre, M. T. A., Arents, J. C., Perez, M. A., van Grondelle, R., Hellingwerf, K. J., and Kennis, J. T. M. (2008) On the signaling mechanism and the absence of photoreversibility in the AppA BLUF domain. *Biophys. J. 95*, 312–321.

BI8010187